18th International Conference on the Application of Computer
Science and Mathematics in Architecture and Civil Engineering
K. Gürlebeck and C. Könke (eds.)
Weimar, Germany, 07–09 July 2009

HYDRO-MECHANICAL COUPLED FIELD SYSTEM IDENTIFICATION - APPLICATION TO WATER RESERVOIRS

T. Lahmer*

**Bauhaus Universität Weimar,*
Research Training Group "Model Validation in Structural Engineering"
Berkaer Str. 9,
99425 Weimar, Germany
E-mail: tom.lahmer@uni-weimar.de

Keywords: Hydro-mechanical coupled fields, water embankments, inverse problem, system identification, crack detection, regularization

Abstract. *It is well known that the precision of the output of any model simulation strongly depends on the caliber of the model parameters. The detection of the model parameters requires generally an adaption of the mathematical model output to certain experimental data. This procedure is referred to as parameter or system identification. Due to the fact that the input data for the inversion has increased measurement inaccuracy, the parameter identification problem needs to be considered as ill-posed and requires appropriate regularization techniques.*
This work concentrates in particular on multi-field problems that occur in structural engineering, e.g. thermo-hydro-mechanical interactions in water dams, embankments or subsoils.
Eventhough the inverse modelling becomes more complex when dealing with multi-physical systems, we expect a better detection of the model parameters due to the correlation of the different measurements.
For example, we consider localized cracks in water dams or fissures in the foundation rock, i.e. irregular material distributions modelled by a smeared crack model. Due to the coupling of different physical fields, the hydraulic head, for instance, influences the stress fields and conversely the mechanical problem affects the hydraulic head. In regions where cracks or fissures are present, i.e. regions of reduced stiffness, the permeability changes, too. Furthermore in regions where the permeability is increased one might expect localized damage zones. Due to the correlation of the measurements, namely hydraulic pore pressure and mechanical displacement at observable points, more information can be gathered compared to the case of considering only single fields. The problem of inaccuracy in the data leads to ill-posed problems and is addressed by appropriate regularizing iterative methods. These methods are used to solve the nonlinear relation between model parameters and measurements in a stable manner. Morozov's discrepancy principle is applied in order to avoid an amplification of errors from the measured data. The trade of between accuracy and stability can be guaranteed.
Numerical results show the effectiveness and convergence properties of the proposed method for a synthetic hydro-mechanical example.

1 INTRODUCTION

In civil engineering construction processes are becoming increasingly supported by simulation models. There are many among these models, where the solutions consist of different physical quantities. For example, numerical models for water dams, embankments and subsoils include the mechanical, hydraulic and thermal fields. The precision of the output of these models depends both on the correct choice of the model and the correct adaption of the model parameters. This article is devoted to an inverse problem for a hydro-mechanical problem, namely the identification of material irregularities within the structures by evaluating both hydraulic and mechanical measurements.

The system identification considered in this article can also be used as a method to monitor an embankment's condition. Undamaged systems have a homogeneous distribution of the material properties according to the construction process. However, damaged systems consist of one or more regions where the material properties differ remarkably within the structure due to partial cracking and elution. Early detection of such damaged zones is essential in order to avoid seepage or even piping.

The article is organized as follows: Section 2 describes a simple case of fluid-solid interaction for small strain situations and a set of partial differential equations is derived. During the third section a numerical scheme for the inverse problem is presented. There, we consider an iterative regularizing scheme which evaluates an adjoint problem during each iteration step. In section 4 numerical results are given.

2 COUPLED FLOW AND SOLID DEFORMATION

Assuming that there is only one phase flow, there are no thermal effects and the system is fully saturated, the simples case of fluid-solid interaction for isotropic materials is derived in the following section. We are aware of the fact that the assumption of full saturation is not perfectly suitable for the simulation of water dams. However we want to keep the representation in this paper as simple as possible and devote the consideration of the Van Genuchten's empiric functions [4] to future research. Since the task of this work is to develop a scheme which is capable of identifying material inhomogeneities this simple approach serves the purpose sufficiently. The hydro-mechanical system is then characterized by the deformation of the solid together with the flow of the fluid through the pores. This kind of coupling is usually referred to as *primary consolidation* in soil mechanics [10]. Setting up the mathematical model of fluid flow-structure interactions involves considering a set of balance and constitutive equations. The following balance equations, the mass balance of liquid (1) and the momentum conservation equation (2), are considered

$$\left(\frac{\alpha - n}{\mathbf{K}_s} + \frac{n}{\mathbf{K}_w}\right)\frac{\partial p}{\partial t} + \alpha \mathbf{m}^T B \frac{\partial \mathbf{u}}{\partial t} + \nabla \cdot \mathbf{q}_{rl} = 0, \tag{1}$$

$$B^T \sigma + \rho_a \mathbf{g} = 0. \tag{2}$$

Here, α is Biot's constant (dimensionless), $\mathbf{K}_s$ and $\mathbf{K}_w$ are the bulk moduli $(\mathrm{N/m^2})$ of the solid and water, respectively. Further $\mathbf{u}$ denotes the mechanical displacement vector (m), p liquid

phase pore pressure ($\mathrm{N/m^2}$), $\mathbf{m}^T = [1,1,1,0,0,0]^T$, n is the porosity and

$$\nabla := \left(\frac{\partial}{\partial x}, \frac{\partial}{\partial y}, \frac{\partial}{\partial z}\right)^T, \quad B := \begin{pmatrix} \frac{\partial}{\partial x} & \cdot & \cdot & \cdot & \frac{\partial}{\partial z} & \frac{\partial}{\partial y} \\ \cdot & \frac{\partial}{\partial y} & \cdot & \frac{\partial}{\partial z} & \cdot & \frac{\partial}{\partial x} \\ \cdot & \cdot & \frac{\partial}{\partial z} & \frac{\partial}{\partial y} & \frac{\partial}{\partial x} & \cdot \end{pmatrix}^T$$

denote the gradient and the strain-displacement differential operators, respectively, see e.g. [10, 7]. The average density $\rho_a := ((1-n)\rho_s + n\rho_w)$ is computed from the densities of solid ρ_s and the fluid ρ_w ($\mathrm{kg/m^3}$). Further, σ denotes the macroscopic total stress tensor ($\mathrm{N/m^2}$) and $\mathbf{g}$ is the acceleration due to gravity ($\mathrm{m/s^2}$). The relative (to the solid) liquid flux $\mathbf{q}_{rw}$ is given by Darcy's law [10, 13] stating that the relative mass flux of the liquid is proportional to the negative gradient of the liquid pore pressure

$$\mathbf{q}_{rw} = -\rho_w \frac{\mathbf{k} k_{rw}}{\mu_w}(\nabla p - \rho_w \mathbf{g}). \tag{3}$$

Here, $\mathbf{q}_{rw}$ ($\mathrm{kg/m^2 s}$) denotes the relative mass flux of the fluid. The isotropic intrinsic permeability tensor is given by $\mathbf{k} := \mathbf{k}_{ij} = \delta_{ij} k$ ($\mathrm{m^2}$). Further k_{rw} is the relative liquid permeability and μ_w the liquid's viscosity ($\mathrm{N/m^2 s}$). The effective stress law for a fully saturated medium is given by

$$\sigma = \sigma'' - \alpha \mathbf{m} p, \tag{4}$$

where σ'' denotes the effective stress tensor.
The latter is computed considering linear elasticity, i.e. $\sigma'' = \mathbf{c} B \mathbf{u}$ where $\mathbf{c} := \mathbf{c}_{ijkl} = \mu\left(\delta_{ik}\delta_{jl} + \delta_{il}\delta_{jk}\right) + \lambda \delta_{ij}\delta_{kl}$ is the modulus of elasticity. The Lamé parameters $\lambda := \frac{\nu E}{(1+\nu)(1-2\nu)}$ and $\mu := \frac{E}{2(1+\nu)}$ are themselves determined by Young's modulus E ($\mathrm{N/m^2}$) and Poisson's ratio ν.
Expressing the theory given above solely in dependence of the unknowns, mechanical displacement $\mathbf{u}$ and liquid pore pressure p, we obtain the following set of partial differential equations

$$\begin{aligned} B^T(\mathbf{c} B \mathbf{u} - \alpha \mathbf{m} p) + \rho_a \mathbf{g} &= 0 \text{ on } \Omega \times [0,T] \\ \left(\frac{\alpha - n}{\mathbf{K}_s} + \frac{n}{\mathbf{K}_w}\right)\frac{\partial p}{\partial t} + \alpha \mathbf{m}^T B \frac{\partial \mathbf{u}}{\partial t} + \nabla \cdot \left(\rho_w \frac{\mathbf{k} k_{rw}}{\mu_w}(-\nabla p + \rho_w \mathbf{g})\right) &= 0 \text{ on } \Omega \times [0,T] \end{aligned} \tag{5}$$

with boundary conditions

$$\begin{aligned} \mathbf{N}^T \sigma &= 0 \text{ on } \partial\Omega \\ \rho_w \frac{\mathbf{k} k_{rw}}{\mu_w}(-\nabla p + \rho_w \mathbf{g}) \cdot \mathbf{n} &= 0 \text{ on } \partial\Omega \\ \mathbf{u}(t) &= 0 \text{ on } \Gamma_3 \\ p(t) &= h(t) \text{ on } \Gamma_4 \\ p(t) &= 0 \text{ on } \Gamma_1 \cup \Gamma_2 \cup \Gamma_5 \end{aligned} \tag{6}$$

and initial conditions

$$\begin{aligned} \mathbf{u}_{|t=0} &= \mathbf{u}_0 \text{ on } \Omega \\ p_{|t=0} &= p_0 \text{ on } \Omega. \end{aligned} \tag{7}$$

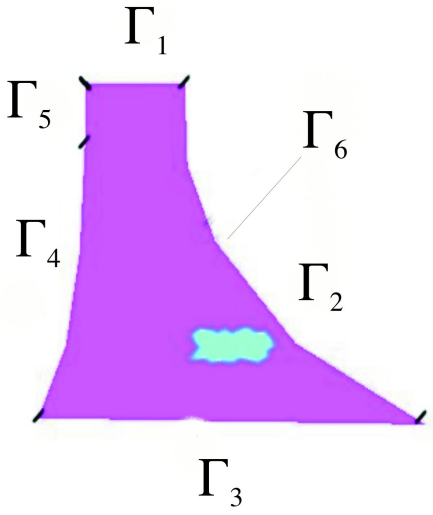

Figure 1: Profile of gravity water dam. The Location of damaged zone is indicated and the boundaries Γ_1 to Γ_5 are labelled, respectively. At the point Γ_6 additional measurements are taken as described in Section 3. The height of the dam modelled is about 29 meters, the crest has a length of 166 meters and the radius of curvature is about 120 meters.

Solving the system in (5) with (6) and (7) will be referred to as *the direct problem*.

In this work a situation of plain strain is considered. The picture in Figure 1 shows the schematic shape of the computational domain Ω, which represents a profile of a gravity water dam. The upstream side is on the left. The decomposition of the boundary into five subboundaries, i.e. $\partial\Omega = \Gamma_1 \cup \Gamma_2 \cup \Gamma_3 \cup \Gamma_4 \cup \Gamma_5$ as indicated. The additionally sketched boundary Γ_6 consists of just one point and is regarded in Section 3 where an additional measurement is taken. The inhomogeneous Dirichlet boundary condition h in (6) is linearly varying with the water depth. A variation in h over time is modelling different filling levels of the water reservoir.

The numerical solution of the forward problem is done with the Finite Element Method. The spatial discretization is performed using standard nodal finite elements. With n_{eq} the number of nodes in the FE-mesh are indicated, on which no homogeneous Dirichlet boundary conditions are defined. Then, the FE approximation for the unknowns is computed as follows

$$\begin{aligned} \mathbf{u} &\approx \mathbf{u}_h = \sum_{k=1}^{n_{eq}} \mathbf{u}_m^k \mathbf{N}_u^k \\ p &\approx p_h = \sum_{k=1}^{n_{eq}} p_m^k N_p^k \end{aligned} \tag{8}$$

where $\mathbf{N}_u$ and N_p are elements of bases of $(S_h)^3$ and T_h which then again are finite dimensional subspaces of $H_0^1(\Omega)$. The nodal displacements and pore pressures $\mathbf{u}_m = (u_m^1, ...u_m^{n_{eq}})$ and $p_m = (p_m^1, ..., p_m^{n_{eq}})$ are now obtained by solving

$$\begin{pmatrix} \mathbf{K} & -\mathbf{Q} \\ 0 & \mathbf{H} \end{pmatrix} \begin{pmatrix} \mathbf{u}_m \\ p_m \end{pmatrix} + \begin{pmatrix} 0 & 0 \\ \mathbf{Q}^T & \mathbf{S} \end{pmatrix} \frac{d}{dt} \begin{pmatrix} \mathbf{u}_m \\ p_m \end{pmatrix} = \begin{pmatrix} f_u \\ f_w \end{pmatrix}$$

where
$\mathbf{Q} = \int_\Omega (B\mathbf{N}_u)^T \alpha \mathbf{m} N_p d\Omega$ is the hydro-mechanical coupling matrix,

$\mathbf{K} = \int_\Omega (B\mathbf{N}_u)^T \mathbf{c} B\mathbf{N}_u d\Omega$ the mechanical stiffness matrix,
$\mathbf{H} = \int_\Omega (\nabla N_p)^T \frac{\mathbf{k}k_{rl}}{\mu} \nabla N_p d\Omega$ the permeability matrix and
$\mathbf{S} = \int_\Omega N_p^T \left(\frac{\alpha - n}{\mathbf{K}_s} + \frac{n}{\mathbf{K}_w} \right) N_p d\Omega$ is the capacity matrix.
For the discretization in time the generalized trapezoidal method, an implicit time stepping scheme is applied, see [10].
Figure 2 shows the pore pressure distribution and the horizontal and vertical component of the mechanical displacement at the final time $t = T$.

3 SYSTEM IDENTIFICATION

This section deals with the *inverse problem*, i.e. the detection of the damaged zone within the dam structure out of combined pore pressure and mechanical displacement measurements. It is assumed that over time the evolution of the mechanical displacement at the tip of the dam and on one point along the downstream side are recorded as follows

$$\mathbf{u}(x,t) = \bar{\mathbf{u}}^\delta(t) \text{ on } \Gamma_u := \Gamma_1 \cup \Gamma_6. \tag{9}$$

Additionally, there are hydraulic pore pressure measurements at the dam's foot available

$$p(x,t) = \bar{p}^\delta(t) \text{ on } \Gamma_p := \Gamma_3. \tag{10}$$

The actual discrete measurements given along the boundaries Γ_1 and Γ_3 are linearly interpolated. This is why we consider measurements along the boundaries and not only along discrete points. Γ_6 consists only of one measurement point along Γ_2, see Figure 1. The hydraulic quantities are recorded by porewater pressure transducers which are located at the dam's foundation. The values obtained from these transducers are used to determine the reduction of the hydraulic potential in the water dam, see e.g. [1]. The mechanical displacements at the crest of the dam and the downstream side are dictated either by plumb line or hanging pendulum (horizontal displacement), geometrical precision differential levelling or geodetic positioning. The superscribed δ in (9) and (10) denotes error components with which measurements are generally contaminated. Whenever the identification is done with noiseless data, the superscribed δ is dropped: $y = y^\delta$ for $\delta = 0$. The δ itself is an L^2 measure of the noise level, i.e. $||y - y^\delta|| < \delta$.

The measurements $\bar{\mathbf{u}}^\delta$ and $\bar{p}^\delta$ are assumed to be functions in $L^2([0,T], L^2(\Gamma_i))$, $i \in \{u, p\}$. The material inhomogeneities are described by a smeared crack model, i.e. the main parameters, Young's modulus and hydraulic conductivity, are described by spatially varying functions with H^1 regularity, i.e.

$$E := E(x) \in H^1(\mathbb{R}^+) \quad \text{and} \quad k := k(x) \in H^1(\mathbb{R}^+). \tag{11}$$

We now define the parameter-to-solution mapping

$$\begin{aligned} F : \mathcal{D}(F) \in V := \{(E,k) \in (H^1(\mathbb{R}^+))^2\} &\rightarrow L^2([0,T], L^2(\Gamma_u)) \times L^2([0,T], L^2(\Gamma_p)) \\ (E(x), k(x)) &\mapsto (\mathbf{u}_{|\Gamma_u}, p_{|\Gamma_p}). \end{aligned} \tag{12}$$

The *inverse problem* with given measured data $y^\delta := (\bar{\mathbf{u}}^\delta, \bar{p}^\delta)$ requires a solution of (12), i.e. an inversion of the parameter-to-solution mapping F. During this inversion one computes values in H^1 out noisy measurements in L^2 which turns by the lack of smoothness in the measured data into an ill-posed problem.

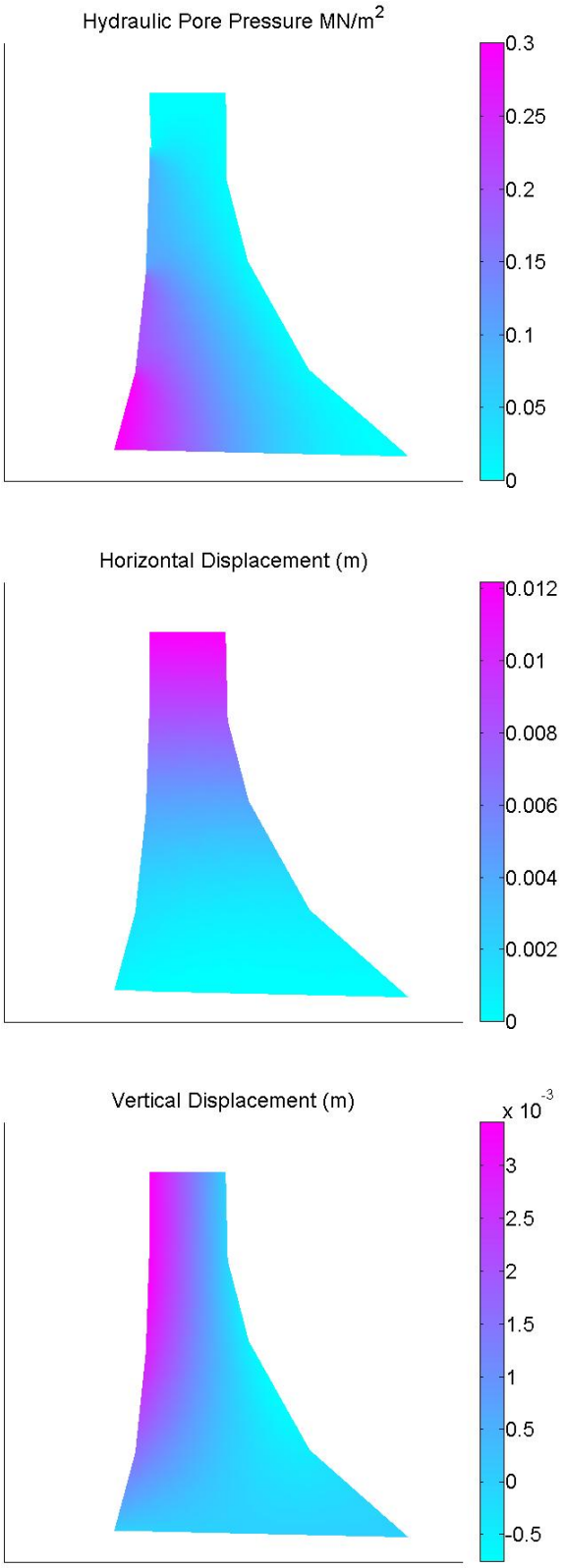

Figure 2: Solution of the forward problem: The first picture shows the distribution of the pore pressure for a fixed time t. The second and third picture plot the mechanical displacement in horizontal and vertical direction, respectively.

For the solution of the inverse problem iterative and regularizing methods are well proven, e.g. the nonlinear Landweber method [5]

$$(E,k)^{n+1,\delta} = (E,k)^{n,\delta} - \omega F'((E,k)^{n,\delta})^* \left(F((E,k)^{n,\delta}) - y^\delta\right). \tag{13}$$

In order to guarantee convergence the relaxation parameter ω in (13) needs to be chosen such that

$$\omega < \frac{1}{||F'((E,k))||}$$

for all $(E,k) \in \mathcal{B}_{2\rho}((E,k)^0)$, where $\mathcal{B}_{2\rho}((E,k)^0)$ denotes a closed ball of radius 2ρ around the initial guess $(E,k)^0$.
Alternatively, one can implement the minimal error method which is a variant of Landweber's iteration with a flexible choice of the relaxation parameter $\omega := \omega^{n,\delta}$ [11, 14] with

$$\omega_i^{n,\delta} := \frac{||F_i((E,k)^{n,\delta}) - y_i^\delta||_{L^2}^2}{||F_i'((E,k)^{n,\delta})^*(F((E,k)^{n,\delta}) - y^\delta)||_{H^1}^2}, \quad i = 1,2, \tag{14}$$

where the additional index i refers to the single parameter field updates. The adjoint of the linearization of F which occurs in (13) applied on a vector (r_u, r_p) is formally given by

$$F'(E,k)^*(r_u,r_p) = \Phi^{-1}\left(\int_0^T \begin{pmatrix} -B\mathbf{u}B\varphi \\ \nabla p \nabla \psi \end{pmatrix} dt\right), \tag{15}$$

where (φ, ψ) are solutions of an *adjoint* system of partial differential equations

$$\begin{aligned}
B^T(\mathbf{c}B\varphi + \alpha\mathbf{m}\frac{\partial\psi}{\partial t}) &= 0 \text{ on } \Omega\times[0,T] \\
-\left(\frac{\alpha-n}{\mathbf{K}_s} + \frac{n}{\mathbf{K}_w}\right)\frac{\partial\psi}{\partial t} - \alpha\mathbf{m}^T B\varphi + \nabla\cdot(\rho_w\frac{\mathbf{k}k_{rw}}{\mu_w}(-\nabla\psi)) &= 0 \text{ on } \Omega\times[0,T] \\
\mathbf{N}^T(\mathbf{c}B\varphi) &= 0 \text{ on } \partial\Omega\setminus\Gamma_u \\
(\rho_w\frac{\mathbf{k}k_{rw}}{\mu_w}(-\nabla\psi))\cdot\mathbf{n} &= 0 \text{ on } \partial\Omega\setminus\Gamma_p \\
\mathbf{N}^T(\mathbf{c}B\varphi) &= r_u \text{ on } \Gamma_u \\
(\rho_w\frac{\mathbf{k}k_{rw}}{\mu_w}(-\nabla\psi))\cdot\mathbf{n} &= r_p \text{ on } \Gamma_p \\
\varphi &= 0 \text{ on } \partial\Omega \\
\psi &= 0 \text{ on } \partial\Omega \\
\varphi_{|t=T} &= 0 \text{ on } \Omega \\
\psi_{|t=T} &= 0 \text{ on } \Omega.
\end{aligned} \tag{16}$$

In (15) the operator Φ is the adjoint of the embedding operator from L^2 into H^1, see e.g. [8]. For a detailed discussion on the computation of an adjoint problem for the identification of the diffusion coefficient in a linear (non coupled) parabolic equation, see [6]. The numerical solution of this adjoint system is also done with the Finite Element Method. Note however, that this system has an end condition, i.e. for $t = T$ and is solved backwards in time.

We define the parameter vector $p := (E, k)$ and set $p^{n,\delta} := (E, k)^{n,\delta}$. In order to avoid an amplification of the data error the iteration in (13) is stopped by a generalized discrepancy principle, i.e. when for the first time

$$||F(p^{n,\delta}) - y^\delta|| \leq \tau\delta, \quad n = 1, 2, ... \tag{17}$$

holds for $\tau > 2$, see [5, 8]. It is shown that an early stopping according to (17) renders the Landweber method a regularizing method [5].

In order to study convergence of the Landweber method, one needs to assume that F is Frèchet-differentiable with $||F'(\cdot)|| \leq 1$ and that $\forall p, \tilde{p} \in \mathcal{B}_\rho(p^0)$:

$$||F(p) - F(\tilde{p}) - F'(p)(p - \tilde{p})|| \leq \eta||F(\tilde{p}) - F(p)||, \quad \eta < \frac{1}{2} \tag{18}$$

holds in $\mathcal{D}(F)$. Then, for any solution $p \in \mathcal{D}(F)$ of $F(p) = y$ a sufficient condition for $p^{n+1,\delta}$ to be a better approximation of the exact solution denoted by $p^\dagger$ is that

$$||y^\delta - F(p^{n,\delta})|| > 2\frac{1+\eta}{1-2\eta}\delta,$$

which gives an estimate on the factor τ in (17). However the condition in (18) can most probably not shown rigorously for the coupled identification problem here. However it is proven to hold for parameter estimation problem in an uncoupled elliptic problem [8] and an harmonic problem in [9].

Convergence rates of Landweber iteration however can only be shown if additionally a source condition of the following type

$$p^\dagger - p^0 = \left(F'(p^\dagger)^* F'(p^\dagger)\right)^\nu w_1, \quad \text{with } \nu > 0 \quad \text{and} \quad w_1 \in \mathcal{N}(F'(p^\dagger))^\perp \tag{19}$$

is fulfilled [5, 8]. The source condition implies a certain smoothness for the difference $p^\dagger - p^0$ for many examples if $\nu > 0$. The rate of convergence can than be shown to be as follows

$$||p^\dagger - p^{n_*(\delta,y^\delta),\delta}|| \leq c_2||w_1||^{\frac{1}{2\nu+1}}\delta^{\frac{2\nu}{2\nu+1}} \tag{20}$$

where the stopping index $n_*(\delta, y^\delta)$ is obtained by (17) and which can be estimated in the following manner

$$n_*(\delta, y^\delta) \leq c_1 \left(\frac{||w_1||}{\delta}\right)^{\frac{2}{2\nu+1}}. \tag{21}$$

For the special case $\nu = \frac{1}{2}$ in (19), the terms in (20) and (21) reduce to

$$\begin{aligned} ||p^\dagger - p^{n_*(\delta,y^\delta),\delta}|| &= \mathcal{O}(\sqrt{\delta}) \\ n_*(\delta, y^\delta) &= \mathcal{O}\left(\frac{1}{\delta}\right). \end{aligned} \tag{22}$$

The condition in (19) means that one has to know all rough parts of the sought-for quantities up to a certain regularity in order to obtain the rate $\mathcal{O}(\sqrt{\delta})$. However the smoothness assumed on the difference $p^\dagger - p^0$ will hardly be fulfilled in the application example given here. Therefore a slower convergence is to expect during the numerical computations.

For the minimal error method convergence rates have only been proven in the case of exact data, i.e. for $\delta = 0$. In this case, for the modified Landweber method with flexible relaxation parameter according to (14), one has

$$||p^n - p^\dagger|| = \mathcal{O}(n^{-\frac{1}{2}}), \tag{23}$$

see e.g. [11].

4 NUMERICAL RESULTS

This section shows numerical results for the identification of the damaged zone in the dam by regarding simultaneously mechanical and hydraulic input data. Synthetically generated data are used as input for the inversion. These data are altered by different amounts of normally distributed noise in order to avoid an inverse crime. The initial guess for the parameter distributions of $E(x)$ and $k(x)$ are constant values and are assumed to hold for the undamaged case. The Figures 3 and 4 show the spatial distribution of the reconstructed Young's modulus and the reconstructed permeability, respectively.

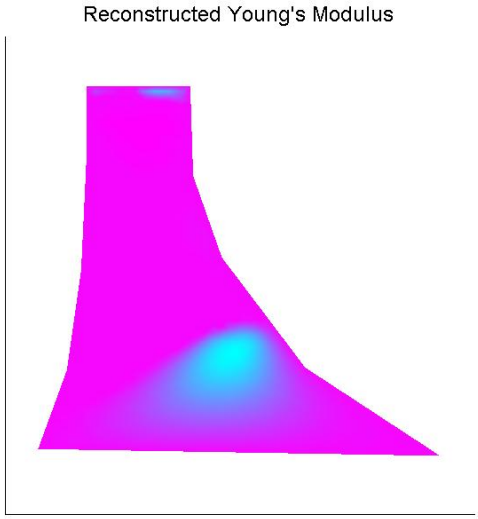

Figure 3: Distribution of Young's modulus after the identification

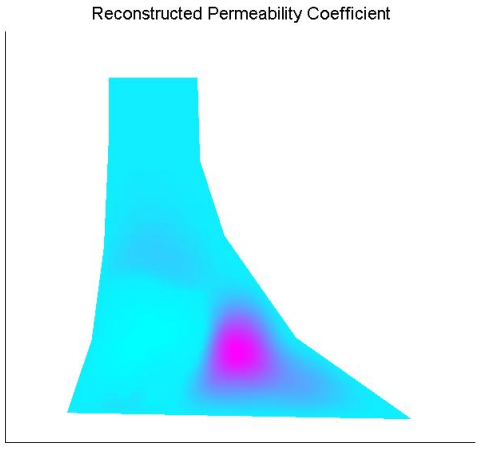

Figure 4: Distribution of permeability after the identification

To this stage, the correlation of the sought-for quantities is not considered yet. Consequently,

two slightly different parameter distributions (which are indicators for the location of the damaged zone) for Young's modulus and the hydraulic conductivity are computed. Looking carefully at Figure 3 it is found that the reconstructed Young's modulus shows a second damaged area close to the boundary Γ_1 at the dam crest. Considering the information from the results of both fields, allows one to mark this second damaged area as irrelevent, since it is not observed for the conductivity, see Figure 4.

Another strategy to combine the information from both field identification is to introduce the following function

$$\chi(x) := \gamma_E E(x) - \gamma_k k(x)$$

with appropriate weighting factors, $\gamma_E > 0$ and $\gamma_k > 0$. These weighting factors are introduced to handle the different orders in magnitude of $E(x)$ and $k(x)$. The function $\chi(x)$ is a weighted mean of information from both fields and provides improved information about the damaged region, see Figure 5. The sharp boundaries around the damaged zone in Figure 6 are obtained by projecting values which exceed (or fall below) a certain value to one (or zero). This threshhold is found by indicating positions where the gradient of χ becomes large, i.e. where a remarkable change in the constitution of the dam is observed.

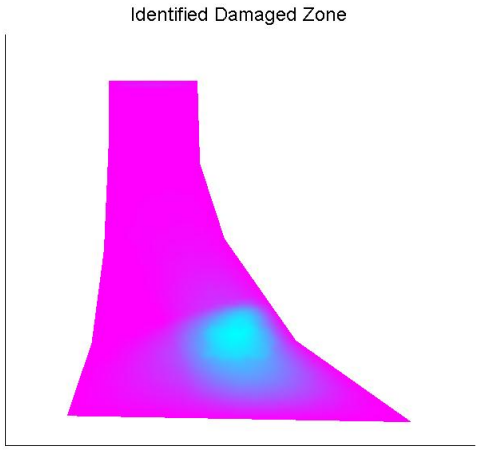

Figure 5: Distribution of the combined variable $\chi(x)$

Numerical computations reveal that the successful identification of material inhomogeneities strongly depends on the location of the inhomogeneity and in particular on the distance between damage and measurements. Obviously a crack close to the tip of the dam is only identified via the mechanical quantities, see Figure 7.

The single mechanical measurement along the boundary Γ_6 turnes out to be indispensable for the identification of the cracked zone considered in both examples. Cracks close to the upstream are observed to be less satisfactorily identifiable than those on the downstream side. This is due to the lack of mechanical measurements under the water. However, these partially discontenting results for this academic example can give valuable hints for a proper placement of the different sensors along or within real-world dam structures. As a consequence the example may be further investigated to answer questions of optimal experiment design for hydro-mechanically coupled problems in civil engineering problems.

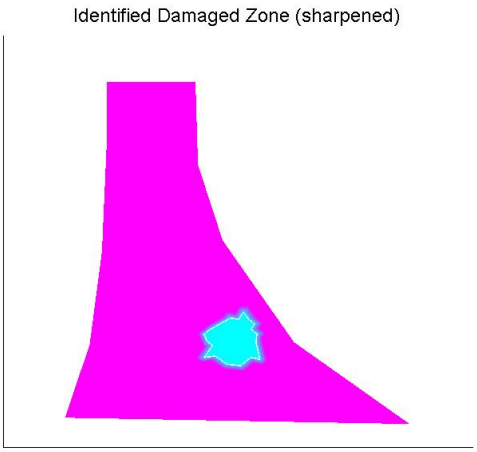

Figure 6: Sharpened solution.

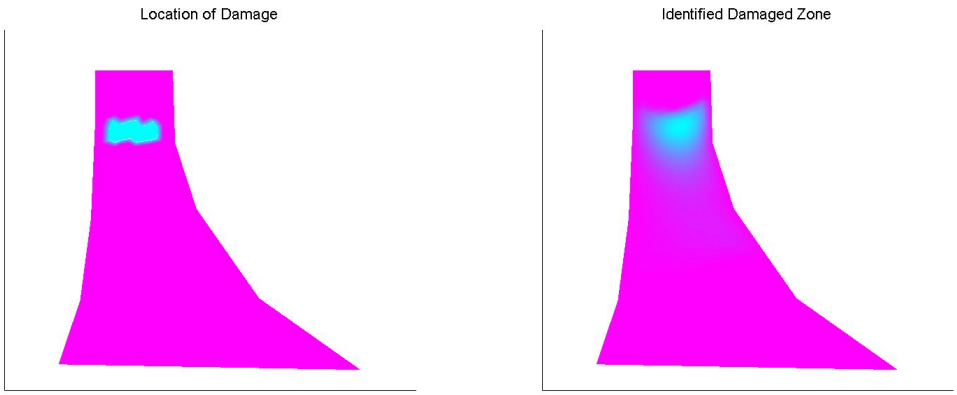

Figure 7: Location and identification of a crack close the the dam's tip.

Finally, results concerning convergence of the implemented scheme in presence of data errors in the measurements are given in Figure 8 and 9. In Figure 8 the norm of the difference between the identified and the exact parameters over an increasing noise level is plotted. Figure 9 shows the decreasing number of iterations for increasing noise level (left). The linear relation between the residual and noise level (right plot) is given by the stopping rule in (17). The numerical convergence results are in accordance with the theory given in equation (22).

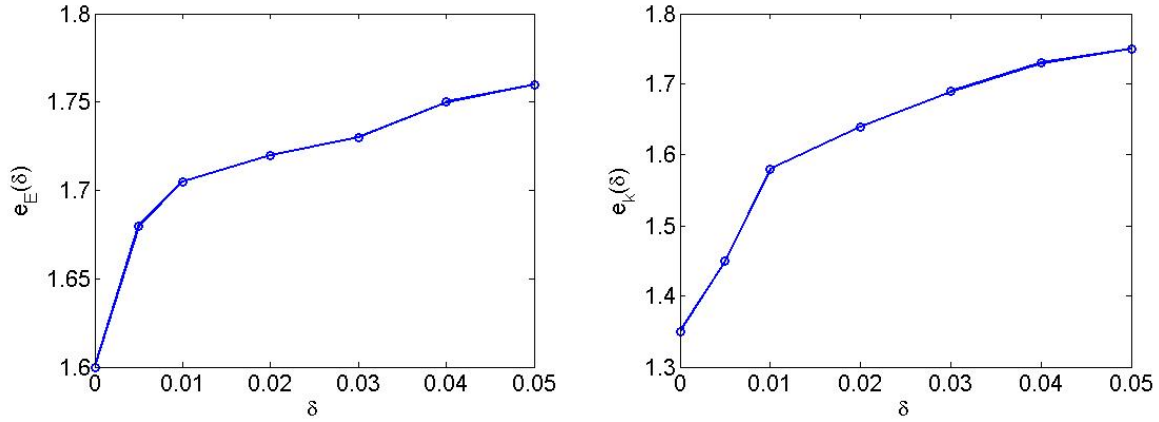

Figure 8: Left: Error $e_E(\delta) := ||E^\dagger - E^{n_*(\delta,y^\delta),\delta}||$ over increasing data noise δ. Right: Error $e_k(\delta) := ||k^\dagger - k^{n_*(\delta,y^\delta),\delta}||$ over increasing data noise δ.

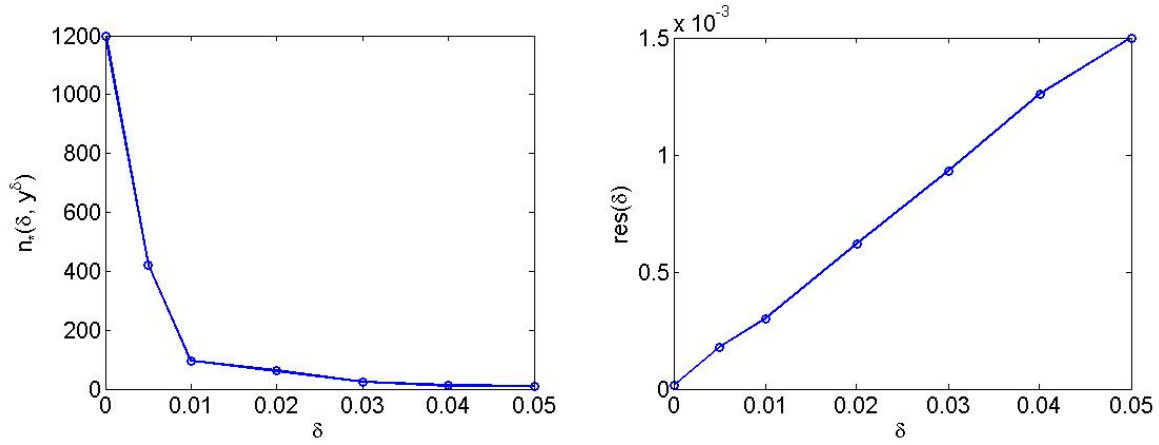

Figure 9: Left: Number of iterations $n_*(\delta, y^\delta)$ for different noise levels δ. Right: Residual $res(\delta) = ||F(p^{n,\delta}) - y^\delta||$ over δ.

5 CONCLUSION AND OUTLOOK

This work presents a numerical scheme for the identification of irregular material distributions in coupled hydro-mechanical systems. The gain in information when evaluating data from the two physical fields involved becomes obvious.

However, one has to be aware that by the small amount of measurements considered, the identification results are not at all regions in the dam as convincing as in the examples shown here. This holds in particular when one regards not only synthetically created data as input for the inversion but in situ observations. In this case, e.g. thermal influences will have strong impacts in particular on the mechanical behavior and need to be regarded in the model. Further, the set of partial differential equations in (5) needs to be extended to model partially saturated media properly.

As already mentioned, the results of this work can further be explored for an optimal experimental design, in other words for answering the questions where to locate sensors and how many sensors are required in order to reliably detect damages in all parts of the structure.

REFERENCES

[1] ASCE Task Committee, *On Guidelines for Instrumentation and Measurements for Monitoring Dam Performance*, American Society of Civil Engineers, (2000).

[2] V. Bettzieche, C. König and C. Könke, *Rissfortschrittsberechnungen beim Standsicherheitsnachweis von Staumauern*, Internationales Symposium Zürich, (2002).

[3] H. W. Engl and M. Hanke and A. Neubauer, *Regularization of Inverse Problems*, Kluwer Dordrecht (1996).

[4] M. Th. van Genuchten, *A Closed-Form Equation for Predicting the Hydraulic Conductivity of Unsaturated Soils*, Soil Sci. Soc. Am. J. **44**, 892-898, (1980).

[5] M. Hanke, A. Neubauer, O. Scherzer, *A convergence analysis of the Landweber iteration for nonlinear ill-posed problem*, Numer. Math 72 (1995), 21-37

[6] A. Hasanov, P. Duchateau, B. Pektacs, *An adjoint problem approach and coarse-fine mesh method for identification of the diffusion coefficient in a linear parabolic equation*, J. Inv. Ill-Posed Problems, Vol 14, No.5, pp 435-463 (2006)

[7] T. J. R. Hughes, *The Finite Element Method, Linear Static and Dynamic FEM*, DOVER PUBLICATIONS, INC. Mineola, New York, (2000).

[8] B. Kaltenbacher, A. Neubauer, O. Scherzer, *Iterative Regularization Methods for Nonlinear Ill-Posed Problems*, Walter de Gruyter GmbH, 2008.

[9] T. Lahmer, *Forward and Inverse Problems in Piezoelectricity*, PhD- Thesis, University of Erlangen-Nuremberg, 2008.

[10] R. W. Lewis, B. A. Schreffler, *The Finite Element Method in the Static and Dynamic Deformation and Consolidation of Porous Media*, Wiley Series in Numerical Methods in Engineering, 1998.

[11] A. Neubauer, O. Scherzer, *A convergent rate result for a steepest descent method and a minimal error method for the solution of nonlinear ill-posed problems*, ZAA 14, 1995

[12] Ruhrverband Essen, Germany, *Sanierung der Fürwiggetalsperre, Abschlussbericht zum Probestau*, 2008.

[13] J. Rutqvist, L. Börgesson, M. Chijimatsu, A. Kobayashi, L. Jing, T. S. Nguyen, J. Noorishad, C.-F. Tsang, *Thermohydromechanics of partially saturated geological media: Governing equations and formulation of four finite element models*, International Journal of Rock Mechanics & Mining Sciences, **38**, 105-127, 2001.

[14] O. Scherzer, *A convergence analysis of a method of steepest descent and a two-step algortihm for nonlinear ill-posed problems*, Numer. Funct. Anal. Optim. 17, (1996), 197-214